JCIM JOURNAL OF CHEMICAL INFORMATION AND MODELING



Computational Chemistry

# Modeling Boronic Acid Based Flourescent Saccharide Sensors: Computational Investigation of d-Fructose Binding to Dimethylaminomethylphenylboronic Acid (DMPBA)

Fiona Kearns, Carrie Robart, Michael T Kemp, Sai Lakshmana Vankayala, Brette M Chapin, Eric Van Anslyn, H. Lee Woodcock, and Joseph D. Larkin

*J. Chem. Inf. Model.*, **Just Accepted Manuscript** • Publication Date (Web): 25 Mar 2019



## Just Accepted



ACS Publications

is published by the American Chemical Society. 1155 Sixteenth Street N.W., Washington, DC 20036

# Modeling Boronic Acid Based Fluorescent Saccharide Sensors: Computational Investigation of d-Fructose Binding to Dimethylaminomethylphenylboronic Acid (DMPBA)

Fiona L. Kearns,[*,†,‖] Carrie Robart,[†,‖] M. Trent Kemp,[†] Sai Lakshmana Vankayala,[†] Brette M. Chapin,[‡] Eric V. Anslyn,[¶] H. Lee Woodcock,[*,†] and Joseph D. Larkin[*,§]

†*Department of Chemistry, University of South Florida, 4202 E. Fowler Ave., CHE205, Tampa, FL 33620-5250, United States*

‡*Department of Chemistry, Durham University, South Road Durham, DH1 3LE, United Kingdom*

¶*Department of Chemistry, The University of Texas at Austin, 100 E 24th Street , Norman Hackerman Building Austin, Texas, 78712, United States*

§*Department of Chemistry, Eckerd College, 4200 54th Ave. South, St. Petersburg, FL 33711, United States*

‖*These two authors contributed equally.*

E-mail: fionakearns@mail.usf.edu; hlw@usf.edu; larkinjd@eckerd.edu

Version as of: March 24, 2019

## Abstract

Designing organic saccharide sensors for use in aqueous solution is a non-trivial endeavor. Incorporation of hydrogen bonding groups on a sensor's receptor unit to target saccharides is an obvious strategy, but not one that is likely to ensure analyte-receptor interactions over analyte-solvent or receptor-solvent interactions. Phenylboronic acids are known to reversibly and covalently bind saccharides (diols in general) with highly selective affinity in aqueous solution. Therefore, recent work has sought to design such sensors and understand their mechanism for allowing fluorescence with bound saccharides. In past work, binding orientations of several saccharides were determined to dimethylaminomethylphenylboronic acid (DMPBA) receptors with an anthracene fluorophore, however the binding orientation of d-fructose to such a sensor could not be determined. In this work, we investigate the potential binding modes by generating 20 possible bidentate and six possible tridentate modes between fructose and DMPBA, a simplified receptor model. Gas phase and implicit solvent geometry optimizations, with a myriad functional/basis set pairs, were carried out to identify the lowest energy bidentate and tridentate binding modes of d-fructose to DMPBA. An interesting hydrogen transfer was observed during selected bidentate gas phase optimizations, this transfer suggests a strong sharing of the hydrogen atom between the boronate hydroxyl and amine nitrogen.

# Introduction:

Carbohydrates are the most abundant class of compounds on Earth and are responsible for a wide variety of crucial roles: cellulose provides structural integrity, starch and glycogen provide energy storage, oligo-saccharides are involved in protein targeting and folding, and controlling cell recognition, and of course d-glucose provides metabolic energy for many organisms.[1–4] Malfunctions in d-glucose regulation in the body are related to many health issues such as obesity, diabetes mellitus,[5] cancer,[6] cystic fibrosis,[7] and renal glycosuria.[8] Thus, having tools to accurately monitor saccharide concentrations in biological solutions and the environment is of great interest to many.

Molecular recognition, binding, and signaling represent a chemist's tools for communicating with analytes at the atomic scale.[9–12] Macromolecules (i.e., proteins, RNA, enzymes) can sequester specific substrates and use concentration information to incite downstream biochemical changes. Chemists, however, have only recently begun systematically targeting analytes through molecular receptors to signal their real-time presence.[13] Synthetic receptors designed to target neutral analytes often exploit intermolecular interactions, such as hydrogen bonding; but in aqueous solution it is challenging to design receptor-analyte interactions that out-compete solvent-analyte interactions.[13]

Saccharides represent a particularly difficult class of compounds to sequester in aqueous solution for many reasons. References 12–32 represent a lengthy, but certainly incomplete, list of past works attempting to tackle this very challenge. The first difficulty in sequestering saccharides is they are structurally complex; for example, the most abundant monosaccharide, d-glucose, has four stereocenters, resulting in a total of 16 stereoisomers. Furthermore, aqueous d-glucose exists in rapid equilibrium between its two cyclized forms, furanose (five membered ring) and pyranose (six membered ring); further still, each of these cyclized forms exists in either an $\alpha$ or $\beta$ anomeric form. Of course, all of d-glucose's related stereoisomers, such as d-fructose, also exist in $\alpha/\beta$–furanose/pyranose forms, each in varying proportions in solution. Not to mention that d-glucose (and its stereoisomers) represent examples of

aldohexose monosaccharides; oligosaccharides and polysaccharides of varying composition greatly exacerbate selectivity problems for molecular receptors.[13]

Additionally, by definition saccharides are poly-hydroxylated alkyl species most often neutral at pH 7.[1,3] Thus, exploiting hydrogen bonding interactions might be one's first instinct when designing an appropriate synthetic receptor for saccharides. However, encouraging saccharide-receptor hydrogen bonding over saccharide-solvent or receptor-solvent hydrogen bonding can be difficult. Nature exploits the hydrophobic effect to overcome this challenge. Examining the crystal structure of *E. coli* glucose/galactose binding protein with bound $\beta$-d-glucopyranose reveals a network of hydrogen bonding residues surrounding $\beta$-d-glucose, and two hydrophobic residues above and below the ring plane. As $\beta$-d-glucose binds, water molecules are expelled to the bulk, resulting in an entropic gain with respect to water.[13,33] Several groups have used this scheme to design molecular receptors which incorporate hydrogen bonding as well as hydrophobic interactions to the carbon-ring, but these designs still do not have high enough association constants to recognize saccharides in biological solution or at dilute concentrations.[12,14,24,34]

It is well established that boronic acids bind to 1,2- and 1,3- diols covalently and reversibly with high affinity in aqueous solution.[35,36] Ever since Lorand and Edward's 1959 demonstration that monosaccharides (d-glucose, d-fructose, D-mannose, and d-galactose) have high affinity for phenylboronic acid (PBA) in aqueous solution,[13,37] much research has been devoted to the use of PBA as the foundation for designing aqueous saccharide receptors.[13,31,32] As shown in Figure 1 in Ref. 20, the covalent and reversible binding of a diol to phenylboronic acid can result through two pathways, either first binding of hydroxyl and release of hydrogen followed by binding of the diol, or by binding of diol then binding of hydroxyl and release of hydrogen.[13]

Photoinduced electron transfer (PET) has long been used in the design of fluorescent sensors for protons and metal ions in solution,[16,17] and has recently been employed in the signaling of saccharides.[15–17,19,25,31,32] In 1994 James, Sandanayake, and Shinkai synthesized

a saccharide receptor and sensor by adding a tertiary amine connected to an anthracene fluorophore as an *ortho* substituent on PBA, see Figure 1 and structures **1** and **2** in Ref. 15. As glucose or fructose were added to an aqueous sensor solution, fluorescence evolved in a manner proportional to saccharide concentration.[15] It was originally hypothesized that binding of saccharide to the sensor induced N–B dative bond formation which prevented nitrogen lone pairs from quenching anthracene fluoresence.[15] Another hypothesis suggested that binding of saccharide increased Lewis acidity of boron, making boron more likely to coordinate a local water molecule, form boronate ester, and release $H^+$.[38,39] In this boronate state, a strong hydrogen bonding interaction could then occur between tertiary nitrogen and the hydroxyl newly bound to boron, thus occupying the nitrogen lone pair and preventing quenching. Other results suggest exciplex formation between fluorophore units is responsible for fluorescence quenching in the unbound state.[40] Saccharide binding to the sensors has been shown to increase sensor solubility and therefore cause disaggregation which allows fluorescence to reemerge.[40] However, in fact, more recent work by Anslyn and coworkers has arrived at a unifying "loose-bolt effect" explanation for the fluorescence mechanism in potentially all *o*-aminomethylphenylboronic acid based saccharide sensors.[41] As Anslyn and coworkers explain, nonradiative decay pathways may emerge via vibrational states accepting electronic excitation energy; thus, high frequency vibrations from the -$B(OH)_3^-$ group can quench fluorescence. However, upon strong binding of fructose, and other 1,2-diols, to *o*-aminomethylphenylboronic acids decreases the number of high frequency vibrational states and therefore decreases potential for this means of vibrational internal conversion, see Ref. 41.

Several groups have illustrated improved synthesis methods of such modular PBA saccharide sensors with tuned specificity for d-glucose.[19,31,32] They were also able to identify the binding modes for d-glucose, l-glucose, and d-galactose, to the receptor, but due to silence on circular dichroism spectra, they were unable to identify the binding mode of d-fructose to the receptor.[31,32] Although Ref 31 was unable to identify a specific d-fructose binding motif

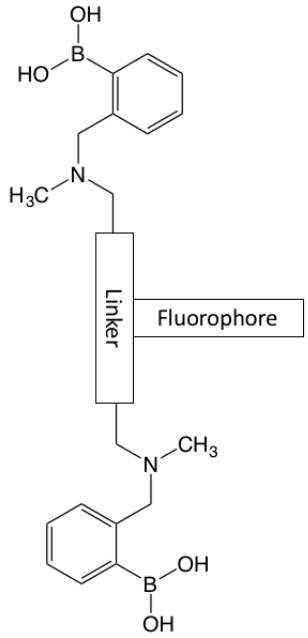


**Figure 1:** Example fluorescent receptor with fluorophore. Sugar binding would take place at phenylboronic acid sites, truncated receptors were modeled in this study.

to the fluorescent sensor, they illustrated that quantum chemical geometry optimzations sufficiently reproduced relative energy trends observed for the other saccharides when binding to a DMPBA model receptor. In order to tune future molecular receptors for the selection of d-fructose, one must know how d-fructose binds to PBA receptors. Towards this end we have conducted an extensive series of quantum mechanical calculations (as done in Ref 31) to identify the most stable fructose isomer with respect to PBA receptor binding, and in what binding orientation. As alluded to, d-fructose exists in solution as an equilibrium between four possible isomers (each at varying concentrations): $\beta$-d-fructopyranose (57-67% in solution), $\alpha$-d-fructopyranose (0-3%), $\beta$-d-fructofuranose (27-31%), $\alpha$-d-fructofuranose (6-9%). Bidentate binding of d-fructose to boron (i.e., two fructose hydroxyls form B–O bonds to boron) may result in five total binding modes per isomer, resulting in 20 total bidentate binding modes between fructose and the PBA receptor. Additionally, each d-fructose isomer may bind to dimethylaminomethylphenylboronic acid (DMPBA) in a tridentate fashion (i.e., three B–O bonds to fructose), as such we have also investigated these six possible structures. Investigating the fluorescence mechanism is outside the scope of this work, therefore to avoid

unnecessary computational expense we have chosen to represent the saccharide sensor in a simplified fashion, only treating dimethylaminephenyl boronic acid, DMPBA. The objective of this work is to identify the most likely fructose binding mode to DMPBA which would aid in designing boronic acid sensors highly selective for d-fructose.

# Methods

**Gas phase optimizations of bidentate complexes:** dimethylaminomethylphenylboronic acid (DMPBA) was taken as a simplified model of the PBA based saccharide receptor, Figure 2. Twenty possible bidentate d-fructose+DMPBA complexes were hypothesized and constructed using ChemDraw 15.0.0, Figure 3. From ChemDraw structures, SMILES codes were obtained for these 20 compounds and the National Cancer Institute's online SMILES translator was used to generate three-dimensional starting structures (`https://cactus.nci.nih.gov/translate/`). Stereochemistry of the starting compounds were visually inspected and verified with VMD (Visual Molecular Dynamics).[42] All QM geometry optimizations were carried out with Q-Chem 4.3.[43]

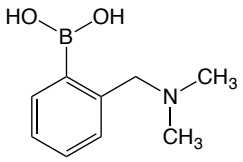


**Figure 2:** Model receptor, dimethylaminomethylphenylboronic acid, DMPBA.

An initial B3LYP/6-31G* geometry optimization was conducted in gas phase for all 20 structures to eliminate bad starting contacts. Given the true binding mode of fructose to DMPBA is not known, and that Larkin et al and others have observed, when modeling bonds to boron, different functional/basis set combinations often predict different relative stabilization energies among bonding patterns, we used a wide variety of functional basis-set pairs to further optimize each potential binding mode.[32,44] Thus, coordinates from the initial optimization were then used for secondary optimizations with the

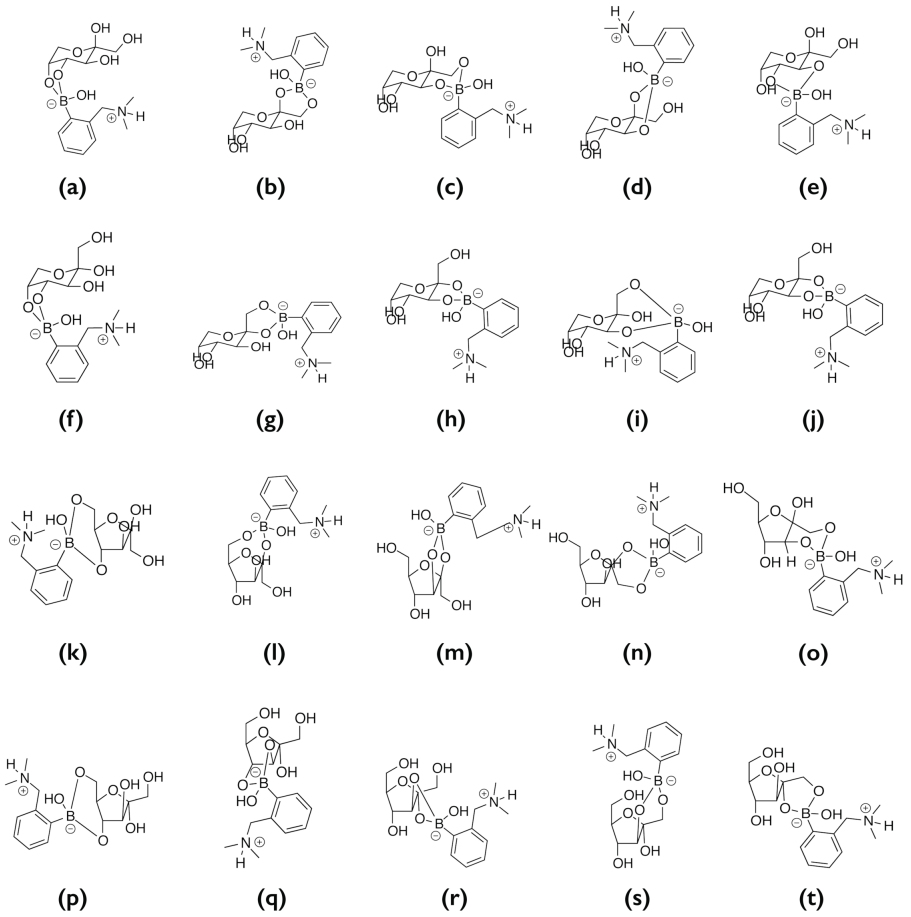


**Figure 3:** All 20 possible bidentate covalent binding modes of d-fructose isomers to DMPBA model fluorescent receptor. For ease of reference, structures have been labeled **a** through **t**. **(a - e)** Row 1: Complexes resulting from $\beta$-d-fructopyranose binding to DMPBA. **(f - j)** Row 2: Complexes resulting from $\alpha$-d-fructopyranose binding to DMPBA. **(k - o)** Row 3: Complexes resulting from $\beta$-d-fructofuranose binding to DMPBA. **(p - t)** Row 4: Complexes resulting from $\alpha$-d-fructofuranose binding to DMPBA.

following functional/basis set pairs: M06-2X/6-31+G*, M06-2X/6-311++G**, $\omega$B97x-D/6-31+G*, $\omega$B97x-D/6-311++G**, PBE/6-31+G*, PBE/6-311++G**, PBE1PBE/6-31+G*, and PBE1PBE/6-311++G**. Final energies were taken from these secondary gas phase optimizations and compared to determine the lowest energy structures.

**Implicit solvent optimizations of bidentate and tridentate complexes:** Following gas phase geometry optimizations, implicit solvent optimizations were conducted to identify how effects of solvent could alter relative energies between the 20 bidentate structures. Solvent Method 8 (SM8) was used to optimize all 20 structures in implicit water. Coordinates were again taken from SMILES translated codes and initially optimized with SM8/$\omega$B97x-D/6-31+G** and SM8/M06-2X/6-311++G** (with "loose" electronic correlation grid, i.e., XC_GRID = 1 and 75,302, respectively). The 7 lowest energy structures from the initial "loose-XC_grid" optimizations were further optimized with SM8/$\omega$B97x-D/6-31+G** and SM8/M06-2X/6-31+G** with tighter grids (75,302 and 99,590, respectively). Final energies from these "tight-grid" optimizations were used to identify the lowest energy structures in implicit solvent.

Six possible tridentate d-fructose+DMPBA binding modes were hypothesized and initially optimized at the $\omega$B97x-D/6-311++G** level of theory in gas phase to clean up bad initial contacts, Figure 4. The loosely optimized structures were then optimized in implicit water at the SM8/$\omega$B97x-D/6-31+G** and SM8/M06-2X/6-31+G** levels with grid sizes of 75,302 and 99,590, respectively.

# Results & Discussion:

Before discussing our results, we would like to comment about the intended scope of this work. In order to accurately compare "binding motifs" of saccharides to a DMPBA model receptor, ideally we would use explicit solvent simulations, in particular QM/MM (quantum mechanical molecular mechanical hybrid modeling) free energy simulations (FES) to account for entropic effects as well. QM/MM FES are incredibly computataionally expensive, and with 26 potential binding modes, calculating the relatively lowest energy binding mode of d-fructose to DMPBA would be intractable. As such, we hope to use the following results from our geometry optimizations to identify those structures which are most likely to contribute

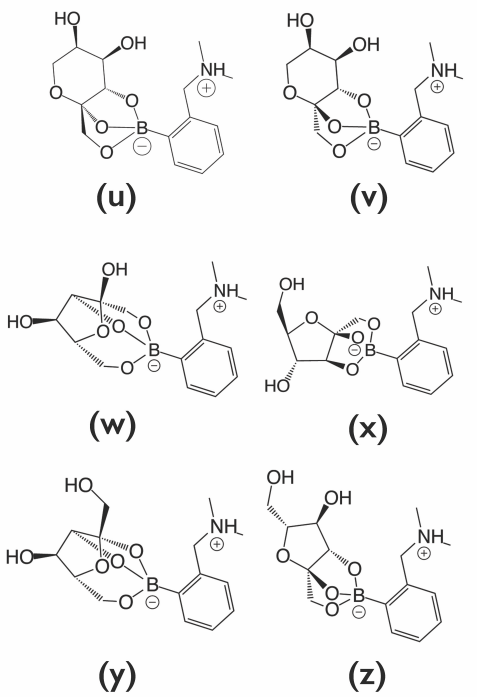


**Figure 4:** All 6 possible tridentate covalent binding modes of fructose isomers to DMPBA model fluorescent receptor. For ease of reference, structures have been labeled **u** through **z**. Structure **u** represents $\beta$-d-fructopyranose binding to DMPBA, **v** represents $\alpha$-d-fructopyranose binding to DMPBA. Structures **w** and **x** represent two possible binding modes for $\beta$-d-fructofuranose to DMPBA. Structures **y** and **z** represent two possible binding modes for $\alpha$-d-fructofuranose binding to DMPBA.

to binding of d-fructose in equilibrium, and then move on to explicit solvent QM/MM FES.

**Gas phase optimizations:** Table 1 indicates there are six low energy binding motifs for fructose isomers in gas phase: **a**, **b**, **c**, **f**, **g**, **n**, with **b** being the lowest in energy. Structure **g** follows close with relative energy differences from **b** between 0.05 – 1.54 kcal·mol$^{-1}$, depending on functional/basis-set. The final structures of the six lowest energy compounds are depicted in Figure 5. Given that **b** represents a binding mode adopted by $\beta$-d-fructopyranose – which is the most abundant fructose isomer in solution at 57-67% – these gas phase data seem to indicate that structure **b** is the most likely fructose binding mode to a DMPBA receptor. However, solvent effects could stabilize other $\beta$-d-fructopyranose binding modes, therefore we also conducted implicit solvent geometry optimizations.

Additionally, an interesting protonation state change was observed over the course of gas phase optimizations. As can be seen in Figure 3, all bidentate binding modes were initially

hypothesized to have tertiary amine $N_{16}$ protonated by $H_{18}$ with $O_{20}$ existing as a hydroxyl bound to boron, see Figure 6 insets for atom numbering. However, after initial B3LYP/6-31G* gas-phase optimizations, the protonation arrangement changed for structures **b**, **f**, and **g**: $H_{18}$, originally protonating $N_{16}$, moved to $O_{20}$ following the initial B3LYP/6-31G* optimization, leaving $N_{16}$ deprotonated and $O_{20}$ doubly protonated and bound to B, with $N_{16}$ and $O_{20}$ tightly sharing $H_{18}$, see Figure 5(b,f,g). As such, we sought to identify the energetic penalties, if any, associated with altering the protonation state of $N_{16}$ and $O_{20}$ in structure **b**. Thus we conducted reaction path mapping studies in gas phase.

**Reaction path mapping in gas phase:** To determine the energetic barrier associated with shifting structure **b**'s $H_{18}$ back to its initial position on $N_{16}$, we conducted a reaction path mapping calculation in Q-Chem 4.3. We did this by using a new feature in QChem's potential energy scan module (PESscan) in which one can specify bonds broken and formed. Here, a defined reaction is carried out by restraining (via force-constant) the selected atom, e.g. $H_{18}$, at various points between the reactant and product states. This restraint is realized by defining a reaction coordinate, $r_{val} = r_1 - r_2$, where $r_1$ is typically the bond to be broken (or lengthened) and $r_2$ is typically the bond to be formed (or shortened). The $r_{val}$ is then varied to "move" the selected atom along the reaction coordinate. For the $H_{18}$ shift from $O_{20}$ to $N_{16}$ in **b**, starting coordinates were taken from the $\omega$B97x-D/6-311++G** optimized structure, 21 steps were conducted at 0.1Å increments to move $r_{val}$ from a value of -0.6Å (-$BOH_2$ N, the reactant state) to 2.0 (-BOH NH, the product state), geometry optimizations were conducted at each step along the reaction coordinate restraining $H_{18}$ at each given $r_{val}$, energies were collected at every step and are shown in Figure 6.

As can be seen in Figure 6, a local maximum was observed along the hydrogen transfer at $r_{val} = 0.0$Å, and a local minimum at $r_{val} = 0.4$Å. The transition state energy (difference in energy between starting state and local maximum, $\Delta E^{\ddagger}$) was calculated to be 1.40 kcal·mol$^{-1}$, while the relative energy between the global and local minima was determined

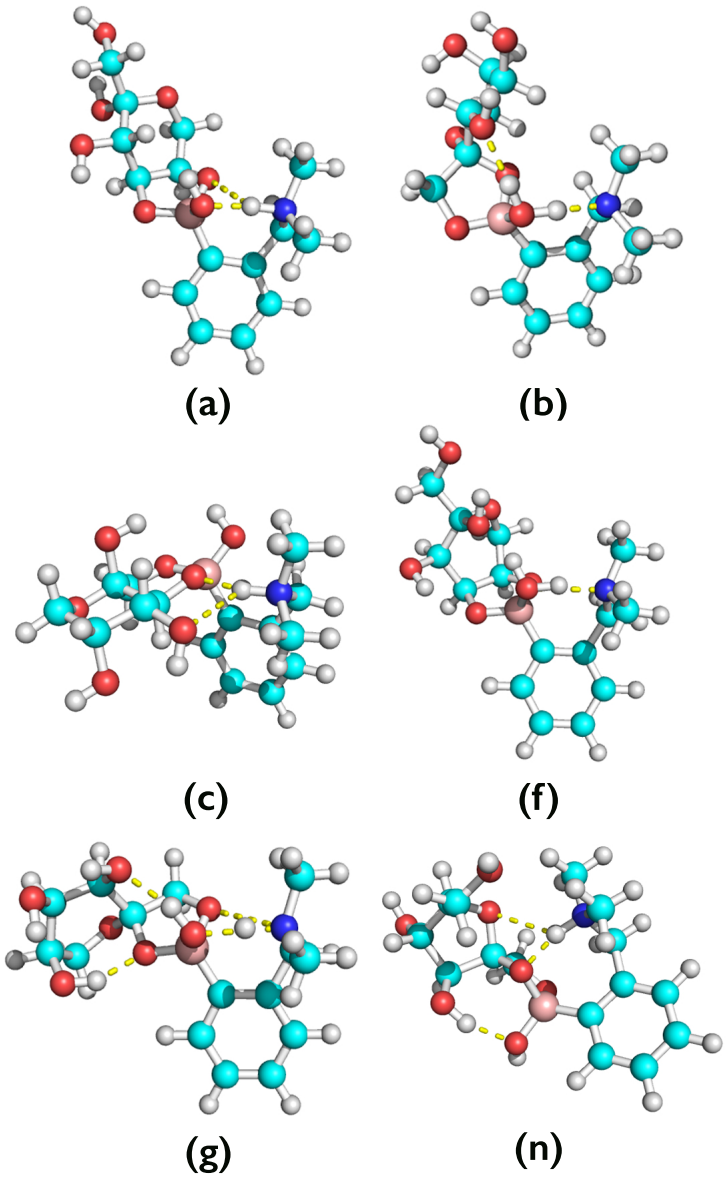


**Figure 5:** Final geometries of 6 lowest energy gas phase structures optimized in gas phase with $\omega$B97x-D/6-31+G**. Optimized gas phase geometries for structures (a) **a**, (b) **b**, (c) **c**, (f) **f**, and (n) **n**.

to be 0.88 kcal·mol$^{-1}$ (it should be noted, the difference in energy between global and local minima is $\sim$ 1.4kT, thus close to thermal energy, potentially indicating significant population at either state). This suggests that the $H_{18}$ could be tightly shared between $O_{20}$ and $N_{16}$. Additionally, the relative energy difference between these two states (O-H vs. N-H) is still smaller than the difference in energy between optimized structures **b** and **g**. Therefore, in gas phase, **b** appears to be the most preferential fructose binding mode, independent of $H_{18}$

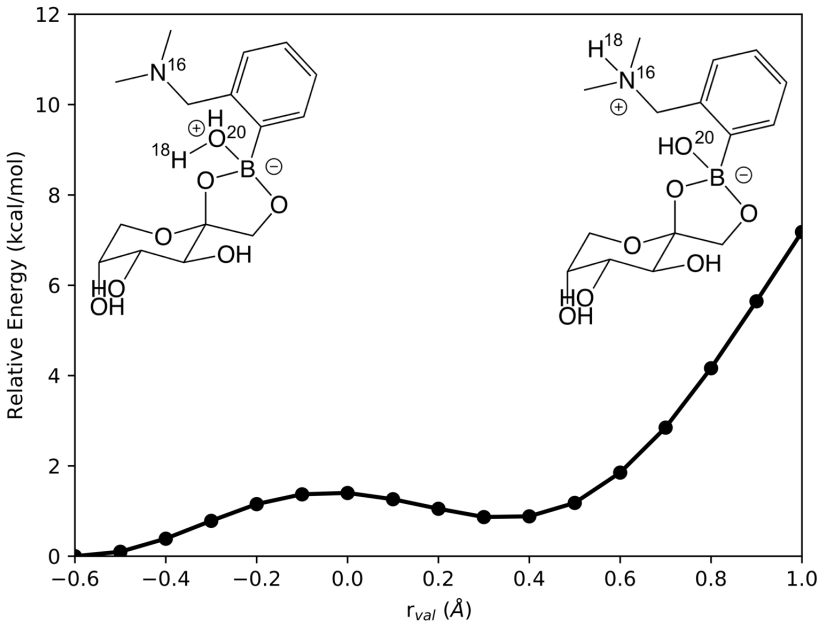


**Figure 6:** Reaction coordinate calculated by moving $H_{18}$ from $O_{20}$ to $N_{16}$ in gas phase. As can be seen, the transition state energy involved in this transformation is 1.4 kcal·mol$^{-1}$ at $r_{val} = 0.0$, and the difference in energy between the global and local minima is 0.88 kcal·mol$^{-1}$.

bonding, with **g** as the second most.

It should also be noted, assuming the PET explanation of fluorescence in these complexes, complete $H_{18}$ transfer from $N_{16}$ to $O_{20}$ (i.e. deprotonation of $N_{16}$) would be contrary to experimentally observed upon fructose binding (as deprotonation would free $N_{16}$'s lone pair and allow quenching of the fluorophore). Thus, we should emphasize that our gas phase optimizations indicate strong sharing of $H_{18}$ between $N_{16}$ and $O_{20}$, which likely would still prevent fluorophore quenching by $N_{16}$ lone pairs, not complete deprotonation. However, this is why thorough investigation is also needed in solvent systems.

**Implicit solvent optimizations:** To identify whether gas phase trends in stability would be consistent in solvent, we conducted implicit solvent geometry optimizations of all 20 structures. SM8 and gas phase optimizations agree with respect to the identity of 7 lowest energy structures – **a**, **b**, **c**, **d**, **f**, **g**, and **n** – however SM8 and gas phase results do not agree with respect to the energetic ordering of these lowest energy structures. Furthermore, within SM8 results there is disagreement between functionals, M06-2X versus $\omega$B97x-D.

Results from SM8/M06-2X/6-31+G** optimizations (Table 2) point to **c** as the most favorable binding mode, followed by **b**, **g**, **f**, **a**, **n**, and **d**. However, SM8/$\omega$B97x-D/6-31+G** points to **g** as the most favored binding mode followed by **b**, **f**, **n**, **c**, **d**, and **a**. Momentarily considering only SM8/M06-2X results, structures **c** and **b**, both $\beta$-d-fructopyranose modes, are predicted to be close in energy, $\Delta_{c/b} = 1.47$ kcal/mol, which is $\sim$ 2.5kT. Thus M06-2X predicts a majority of d-fructose binding could be represented by structure **c** with potentially non-negligible contribution from structure **b**. However, according to SM8/$\omega$B97x-D, structures **b** and **c** are much closer in energy with $\Delta_{c/b} = 0.36$ kcal/mol $<$ thermal energy, possibly indicating equal contribution from **b** and **c** in solution. Therefore, although SM8/M06-2X and SM8/$\omega$B97x-D do not strictly agree on energetic trends they do agree structures **b** and **c** are both likely binding modes in solution. Furthermore, SM8/$\omega$B97x-D results indicate stable d-fructose binding to DMPBA could result from several orientations, possibly explaining the difficulty in experimentally resolving the structure. However, the two methods do not agree on overal ranking of the lowest energy structures. If one calculates the difference energy between methods for **b**, **c**, and **g**, 0.52 kcal/mol, 1.31 kcal/mol, and 1.77 kcal/mol, respectively,[45] illustrate an average inter-method $\Delta\Delta E$ of 1.2 kcal/mol. This energetic disagreement between methods for the lowest energy 3 structures is $< \Delta_{g/b}(\omega$B97x-D$) = 0.95$ kcal/mol and $\sim \Delta_{g/c}(\omega$B97x-D$) = 1.31$ kcal/mol. Considering this, structures **b**, **c**, and **g** could be considered isoenergetic when measured in SM8 water. Images of the SM8 optimized bidentate structures can be seen in Figure 7.

Interestingly, SM8 optimizations did not illustrate the same $H_{18}$ transfer from $N_{16}$ to $O_{20}$ as was observed for gas phase optimizations. To test the penalties, if any, for transferring $H_{18}$ in the presence of solvent, we also conducted reaction path mapping with SM8 water.

**Reaction path mapping in SM8 water:** As can be seen in Figure 7, after optimization in SM8 water, the $H_{18}$ transfer from $N_{16}$ to $O_{20}$ as seen in gas phase for bidentate structures **b**, **f**, and **g** was not observed. To understand why $H_{18}$ would transfer to $O_{20}$ in gas but not

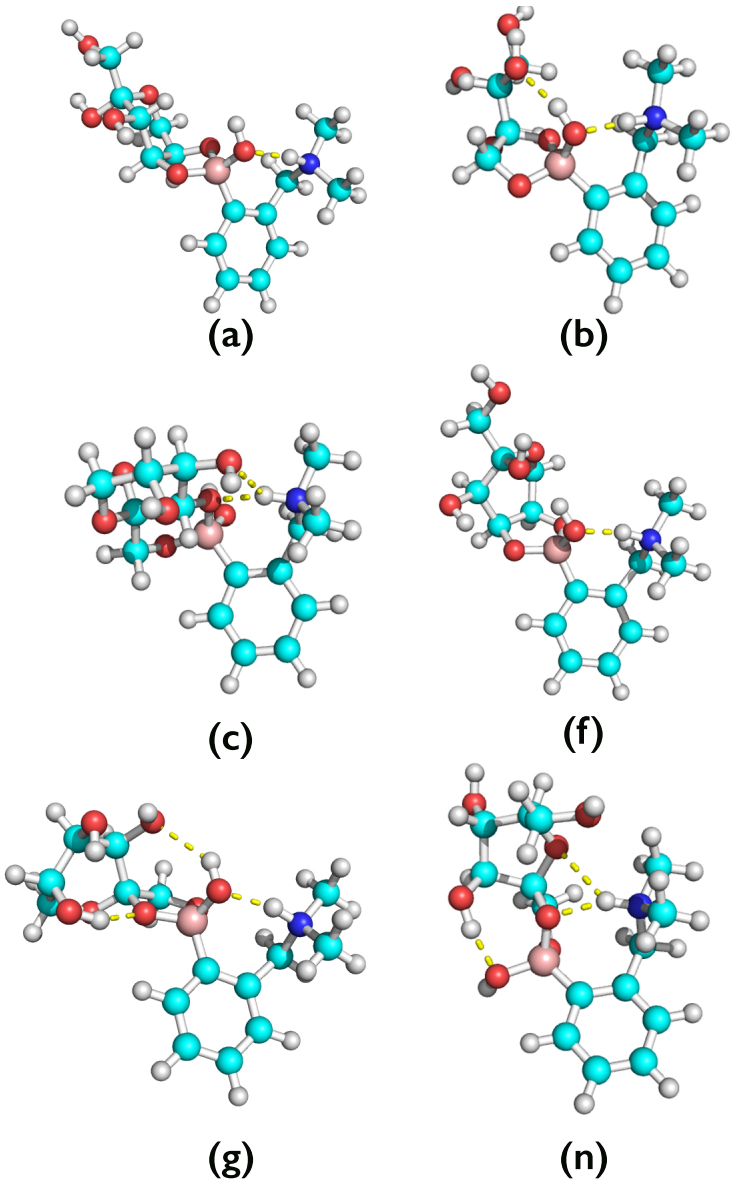


**Figure 7:** Final geometries of 6 lowest energy gas phase structures optimized with SM8/ωB97x-D/6-31+G**. Optimized SM8 geometries for structures (a) **a**, (b) **b**, (c) **c**, (f) **f**, and (n) **n**.

solvent, we estimated energetic penalties along this path again using reaction path mapping. To do so, we took structure **b** gas phase reaction coordinates and re-optimized with SM8 implicit water, leaving the appropriate $r_{val}$ distance constraint on $N_{16}$, $O_{20}$, and $H_{18}$ atoms. Figure 8 shows the energy along this path, $r_{val}$ = -0.6Å corresponds to -$BOH_2$ N bonding as seen in gas phase optimized **b**, and $r_{val}$ = 0.6 Å corresponds to -BOH NH bonding as seen in the initial structures generated from ChemDraw 15.0.0 and as seen in final optimized SM8

structures ($r_{val} > 0.6$ indicates shortening N-H bond beyond its equilibrium value). There is a low energy minimum along this path at $r_{val} = 0.6$Å, which corresponds to an N–H distance of 1.05 Å, close to the equilibrium value. As can be seen, attempting to abstract $H_{18}$ from $N_{16}$ in SM8 (i.e., moving from $r_{val} = 0.6$ to $r_{val} = -0.6$) results in a large energy spike, and thus $H_{18}$ transfer does not appear likely in solution.

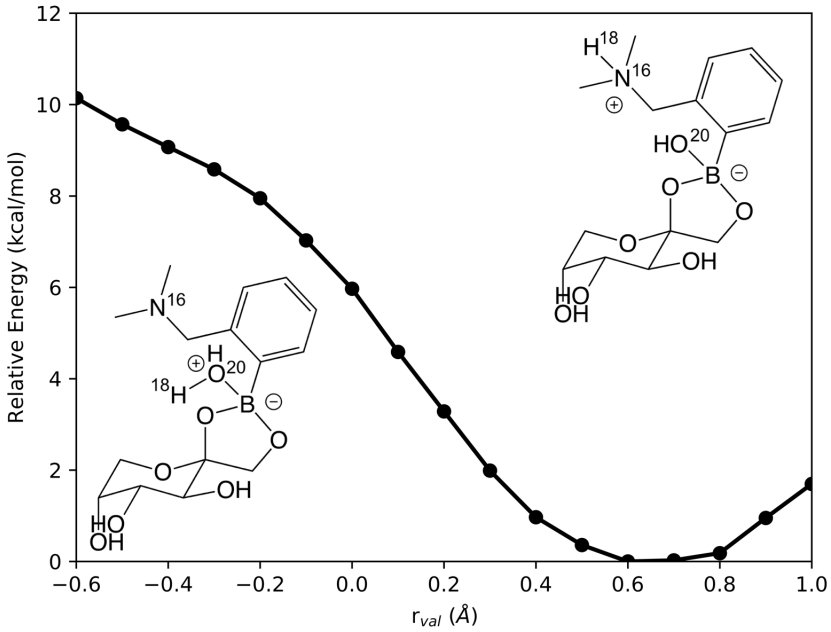


**Figure 8:** Reaction coordinate calculated by modeling the transfer of $H_{18}$ between $O_{20}$ and $N_{16}$. $R_{val}$ = -0.6 would indicate -$BOH_2$ N bonding, while $r_{val} = 0.6$ indicates -BOH NH bonding, $r_{val} > 0.6$ indicates shortening of NH bond beyond equilibrium value. Structures were taken from gas phase reaction path optimizations $H_{18}$ transfer optimizations and reoptimized with SM8/$\omega$B97x-D/6-31++G**. As can be seen, there is an energy minimum at $r_{val} = 0.6$, which corresponds to an NH bond distance of 1.05 Å, which is seen in the SM8 geometry optimized structure. Thus, under the influence of SM8 water, hydrogen transfer from $N_{16}$ to $O_{20}$ is not likely, unlike gas phase results.

It is not too surprising that H-transfer in vacuo appears likely/probable, but not so in implicit solvent. Without the influence of a dielectric constant, strongly polarized neighboring groups may seak energetic minima via intramolecular interactions. In implicit solvent, however, such electrostatic interactions will likely be weakened. However, utilizing an explicit solvent model – which would provide change in dielectric as well as approximate entropic contributions, and hydrogen bonding networks – could lower the barrier to H transfer in solvent, despite implicit solvent results. As such, it will be important to investigate potential H

transfer in future explicit solvent simulations. Furthermore, given that H transfer in implicit solvent does not appear likely, saccharide binding to the fluorescent receptor could induce strengthening of the N-H bond, and therefore prevent quenching by N, however TD-DFT calculations would be required to resolve this hypothesis, and other research suggests the fluorescence mechanism relies on vibrational-electronic coupling (i.e. the "loose-bolt" effect).

**Implicit solvent tridentate binding modes:** Tridentate binding modes for d-fructose isomers were also explored with SM8 water optimizations. Table 3 shows the relative energies for the six possible tridentate binding modes in kcal·mol$^{-1}$, visualized in Figures 4 and 9. Both $\omega$B97x-D and M06-2X results predict structure **w** as the lowest energy structure followed by **y**, **u**, **v**, and finally **z**. Structure **w** is a $\beta$-d-fructofuranose (27-31%) binding mode and thus it is relatively populated in solution. However, structure **u** represents binding of $\beta$-d-fructopyranose, a more likely isomer in solution at 57-67%; $\Delta_{w/u}$ is large, $\sim$ 6 kcal/mol, which is nearly 3 times thermal energy at 2.4 kcal/mol. One could therefore consider since the binding energy difference is large, and since there is a large difference in solution population between furanose and pyranose forms that perhaps tridentate modes would be unlikely. However, the difference between bidentate and tridentate binding modes would largely come down to entropic contributions as a result of releasing another water molecule into solution. As such, we cannot yet rule out tridentate modes **w**, **y**, and **u** as providing significant contributions to d-fructose/DMPBA binding. In future work we plan to conduct free energy simulations to calculate relative free energies between these tridentate complexes as well as between tridentate complexes and bidentate complexes. Again, this result potentially indicates why experimental resolution of the fructose binding to DMPBA is difficult: many different motifs are likely.

# Conclusions

Gas phase geometry optimizations predict structure **b** to be the lowest energy bidentate fructose binding mode to DMPBA and illustrated an interesting $H_{18}$ transfer from $N_{16}$ to $O_{20}$ in structures **b**, **g**, and **f**; however reaction path optimization results indicate that $H_{18}$ is still tightly bound between both $O_{20}$ and $N_{16}$. Implicit solvent optimizations with M06-2X and $\omega$B97x-D predict that structures **a**, **b**, **c**, **d**, **f**, **g**, and **n** are the lowest energy bidentate structures, compared to the other 13 structures, a prediction that is in agreement with gas phase results. However, implicit solvent optimizations point to either **c** or **b** as the lowest energy bidentate binding modes (considering only $\beta$-d-fructopyranose modes). However, SM8/$\omega$B97x-D results indicate potential for **c** and **b** to exist in solution in similar populations as they are very close in energy. Finally, SM8 geometry optimizations indicate **w**, a $\beta$-d-fructofuranose binding mode, to be the most favored tridentate binding mode with the next most favorable binding mode being **u**. However, given $\beta$-d-fructofuranose is less frequent in solution relative to $\beta$-d-fructopyranose, and given **u** is $\sim$ 6 kcal/mol higher in energy (three times thermal energy) than **w**, we predict tridentate binding modes for fructose to DMPBA may not be as likely as bidentate binding modes.

# Supporting Information Available

Interested readers can find all of our QChem 4.3 input and output files (for all molecules optimized with all method/basis set combinations) at the following Zenodo link: `https://doi.org/10.5281/zenodo.2592829`.

# Acknowledgement

The authors would like to thank the University of South Florida Department of Chemistry, University of South Florida Research Computing, NSF, NIH, Pletnev and co-workers, Tom

Holmes group. HLW and JDL would like to thank the National Heart, Lung, and Blood Institute of the National Institutes of Health (Grant K22HL113045) for support. Additionally, H.L.W. would like to highlight that this material is based upon work supported by the National Science Foundation under CHE-1464946. FLK would also like to thank NSF GRFP (project number 3900101301) for support. EVA would like to thank support from the Welch Regents Chair (F-0045). Finally, FLK, CR, and HLW would like recognize additional computational support was provided, through collaboration with University of South Florida's Computing Cluster (CIRCE) team, via NSF's Major Research Instrumentation Program (MRI-1531590).

# References

(1) Lehninger, A.; Nelson, D. L.; Cox, M. M. *Lehninger Principles of Biochemistry*, 5th ed.; W. H. Freeman: New York, NY, 2008.

(2) Collins, P. M.; Ferrier, R. J. *Monosaccharides: Their Chemistry and Their Roles in Natural Products*; John Wiley and Sons, Ltd.: West Sussex, 1995.

(3) Garrett, R. H.; Grisham, C. M. *Biochemistry*; Saunders College Publishing: Fort Worth, 1999.

(4) Dwek, R. A.; Butters, T. D. Introduction: Glycobiology Understanding the Language and Meaning of Carbohydrates. *Chem. Rev.* **2002**, *102*, 283–284.

(5) Wild, S. H.; Roglic, G.; Green, A.; Sicree, R.; King, H. Global Prevalence of Diabetes: Estimates for the Year 2000 and Projections for 2030 - Response to Rathman and Giani. *Diabetes Care* **2004**, *27*, 2569.

(6) Yamamoto, T.; Seino, Y.; Fukumoto, H.; Koh, G.; Yano, H.; Inagaki, N.; Yamada, Y.; Inoue, K.; Manabe, T.; Imura, H. Over-expression of Facilitative Glucose Transporter Genes in Human Cancer. *Biochem. Biophys. Res. Comm.* **1990**, *170*, 223 – 230.

(7) Baxter, P.; Goldhill, J.; Hardcastle, J.; Hardcastle, P. T.; Taylor, C. J. Enhanced Intestinal Glucose and Alanine Transport in Cystic Fibrosis. *Gut* **1990**, *31*, 817–820.

(8) de Marchi, S.; Cecchin, E.; Basil, A.; Proto, G.; Donadon, W.; Jengo, A.; Schinella, A.; Jus, A.; Villalta, D.; De Paoli, P.; Santini, G.; Tesio, F. Close Genetic Linkage between HLA and Renal Glycosuria. *J. Neph.* **1984**, *4*, 280–286.

(9) Czarnik, A. W., Ed. *Fluorescent Chemosensors for Ion and Molecule Recognition*; American Chemical Society: Bonas, 1993; Vol. 538.

(10) de Silva, A. P.; Nimal Gunaratne, H. Q.; Gunnlaugsson, T.; Huxley, A. J. M.; McCoy, C. P.; Rademacher, J. T.; Rice, T. E. Signaling Recognition Events with Fluorescent Sensors and Switches. *Chem. Rev.* **1997**, *97*, 1515–1566.

(11) Hartley, J. H.; James, T. D.; Ward, C. J. Synthetic Receptors. *J. Chem. Soc., Perkin Trans. 1* **2000**, 3155–3184.

(12) Davis, A. P.; James, T. D. In *Functional Receptors*; Schrader, T., Hamilton, A. D., Eds.; Blackwell Science Publishing, Osney Mead: Oxford, 2005; pp 45–109.

(13) James, T. D.; Phillips, M. D.; Shinkai, S. In *Boronic Acids in Saccharide Recognition*; Stoddart, J. F., Ed.; Monographs in Supramolecular Chemistry; The Royal Society of Chemistry: Cambridge, 2006; pp i–174.

(14) Aoyama, Y.; Tanaka, Y.; Toi, H.; Ogoshi, H. Polar Host-Guest Interaction. Binding of Nonionic Polar Compounds with a Resorcinol-aldehyde Cyclooligomer as a Lipophilic Polar Host. *J. Am. Chem. Soc.* **1988**, *110*, 634–635.

(15) James, T. D.; Sandanayake, K. R. A. S.; Shinkai, S. A Glucose-Selective Molecular Fluorescence Sensor. *Ang. Chem. Int. Ed.* **1994**, *33*, 2207–2209.

(16) James, T. D.; Linnane, P.; Shinkai, S. Fluorescent Saccharide Receptors: a Sweet

Solution to the Design, Assembly and Evaluation of Boronic Acid Derived PET Sensors. *Chem. Commun.* **1996**, 281–288.

(17) James, T. D.; Samanjumara Sandanayake, K. R. A.; Shinkai, S. Saccharide Sensing with Molecular Receptors Based on Boronic Acid. *Ang. Chem. Int. Ed.* **1996**, *35*, 1910 –1922.

(18) James, T. D.; Shinkai, S. In *Host-Guest Chemistry: Mimetic Approaches to Study Carbohydrate Recognition*; Penadés, S., Ed.; Springer Berlin Heidelberg: Berlin, Heidelberg, 2002; pp 159–200.

(19) Arimori, S.; Bell, M. L.; Oh, C. S.; Frimat, K. A.; James, T. D. Modular Fluorescence Sensors for Saccharides. *J. Chem. Soc., Perkin Trans. 1* **2002**, 803–808.

(20) Bosch, L.; Fyles, T.; James, T. Binary and Ternary Phenylboronic Acid Complexes with Saccharides and Lewis Bases. *Tetrahedron* **2004**, *60*, 11175 – 11190, Synthetic Receptors as Sensors.

(21) James, T. D.; Shinkai, S. *Advanced Concepts in Fluorescence Sensing Part B: Macromolecular Sensing*; Springer-Verlag: Berlin, Heidelberg, 2005; pp 41–67.

(22) Fossey, J. S.; James, T. D. In *Reviews in Fluorescence*; Geddes, C. D., Ed.; Springer: Berlin, Heidelberg, 2009; pp 103–118.

(23) James, T. D. In *Creative Chemical Sensor Systems. Topics in Current Chemistry, vol 277.*; Schrader, T., Ed.; Springer: Berlin, Heidelberg, 2007; pp 107–152.

(24) Davis, A. P.; Wareham, R. S. A Tricyclic Polyamide Receptor for Carbohydrates in Organic Media. *Ang. Chem. Int. Ed.* **1998**, *37*, 2270–2273.

(25) Sharrett, Z.; Gamsey, S.; Hirayama, L.; Vilozny, B.; Suri, J. T.; Wessling, R. A.; Singaram, B. Exploring the Use of APTS as a Fluorescent Reporter Dye for Continuous Glucose Sensing. *Org. Biomol. Chem.* **2009**, *7*, 1461–1470.

(26) Shimpuku, C.; Ozawa, R.; Sasaki, A.; Sato, F.; Hashimoto, T.; Yamauchi, A.; Suzuki, I.; Hayashita, T. Selective Glucose Recognition by Boronic Acid Azoprobe/[gamma]-cyclodextrin Complexes in Water. *Chem. Commun.* **2009**, 1709–1711.

(27) Yu, C.; Yam, V. W.-W. Glucose Sensing via Polyanion Formation and Induced Pyrene Excimer Emission. *Chem. Commun.* **2009**, 1347–1349.

(28) Cui, Q.; Ward Muscatello, M. M.; Asher, S. A. Photonic Crystal Borax Competitive Binding Carbohydrate Sensing Motif. *Analyst* **2009**, *134*, 875–880.

(29) Ma, W. M. J.; Pereira Morais, M. P.; D'Hooge, F.; van den Elsen, J. M. H.; Cox, J. P. L.; James, T. D.; Fossey, J. S. Dye Displacement Assay for Saccharide Detection with Boronate Hydrogels. *Chem. Commun.* **2009**, 532–534.

(30) Jin, S.; Cheng, Y.; Reid, S.; Li, M.; Wang, B. Carbohydrate Recognition in Boonolectins, Small molecules, and Lectins. *Medical Research Reviews 30*, 171–257.

(31) Larkin, J. D.; Frimat, K. A.; Fyles, T. M.; Flower, S. E.; James, T. D. Boronic Acid Based Photoinduced Electron Transfer (PET) Fluorescence Sensors for Saccharides. *New J. Chem.* **2010**, *34*, 2922–2931.

(32) Larkin, J. D.; Fossey, J. S.; James, T. D.; Brooks, B. R.; Bock, C. W. A Computational Investigation of the NitrogenBoron Interaction in o-(N,N-Dialkylaminomethyl)arylboronate Systems. *J. Phys. Chem. A* **2010**, *114*, 12531–12539, PMID: 21050022.

(33) Vyas, N. K.; Vyas, M. N.; Quiocho, F. Sugar and Signal-Transducer Binding Sites of the *Escherichia coli* Galactose Chemoreceptor Protein. *Science* **1988**, *242*, 1290–1295.

(34) Davis, A. P.; Wareham, R. S. Carbohydrate Recognition through Noncovalent Interactions: A Challenge for Biomimetic and Supramolecular Chemistry. *Ang. Chem. Int. Ed.* **1999**, *38*, 2978–2996.

(35) Boeseken, J. Über die Lagerung der Hydroxyl-Gruppen von Polyoxy-Verbindungen im Raum. Die Konfiguration der gesättigten Glykole und der $\alpha$- und $\beta$-Glykose. *Berichte* **1913**, *46*, 2612–2628.

(36) Boeseken, J. The Use of Boric Acid for the Determination of the Configuration of Carbohydrates. *Adv. Carb. Chem.* **1949**, *4*, 189–210.

(37) Lorand, J. P.; Edwards, J. O. Polyol Complexes and Structure of the Benzeneboronate Ion. *J. Org. Chem.* **1959**, *24*, 769–774.

(38) Franzen, S.; Ni, W.; Wang, B. Study of the Mechanism of Electron-Transfer Quenching by Boron–Nitrogen Adducts in Fluorescent Sensors. *J. Phys. Chem. B* **2003**, *107*, 12942–12948.

(39) Ni, W.; Kaur, G.; Springsteen, G.; Wang, B.; Franzen, S. Regulating the Fluorescence Intensity of an Anthracene Boronic Acid System: a B-N Bond or a Hydrolysis Mechanism? *Bioorg. Chem.* **2004**, *32*, 571581.

(40) Chapin, B. M.; Metola, P.; Vankayala, S. L.; Woodcock, H. L.; Mooibroek, T. J.; Lynch, V. M.; Larkin, J. D.; Anslyn, E. V. Disaggregation is a Mechanism for Emission Turn-On of ortho-Aminomethylphenylboronic Acid-Based Saccharide Sensors. *J. Am. Chem. Soc.* **2017**, *139*, 5568–5578, PMID: 28358506.

(41) Sun, X.; James, T. D.; Anslyn, E. V. Arresting Loose Bolt Internal Conversion from B(OH)2 Groups is the Mechanism for Emission Turn-On in ortho-Aminomethylphenylboronic Acid-Based Saccharide Sensors. *J. Am. Chem. Soc.* **2018**, *140*, 2348–2354, PMID: 29360350.

(42) Humphrey, W.; Dalke, A.; Schulten, K. VMD – Visual Molecular Dynamics. *J. Molec. Graph.* **1996**, *14*, 33–38.

(43) Shao, Y.; Gan, Z.; Epifanovsky, E.; Gilbert, A. T.; Wormit, M.; Kussmann, J.; Lange, A. W.; Behn, A.; Deng, J.; Feng, X.; Ghosh, D.; Goldey, M.; Horn, P. R.; Jacobson, L. D.; Kaliman, I.; Khaliullin, R. Z.; Kuś, T.; Landau, A.; Liu, J.; Proynov, E. I.; Rhee, Y. M.; Richard, R. M.; Rohrdanz, M. A.; Steele, R. P.; Sundstrom, E. J.; Woodcock, H. L.; Zimmerman, P. M.; Zuev, D.; Albrecht, B.; Alguire, E.; Austin, B.; Beran, G. J. O.; Bernard, Y. A.; Berquist, E.; Brandhorst, K.; Bravaya, K. B.; Brown, S. T.; Casanova, D.; Chang, C.-M.; Chen, Y.; Chien, S. H.; Closser, K. D.; Crittenden, D. L.; Diedenhofen, M.; DiStasio, R. A.; Do, H.; Dutoi, A. D.; Edgar, R. G.; Fatehi, S.; Fusti-Molnar, L.; Ghysels, A.; Golubeva-Zadorozhnaya, A.; Gomes, J.; Hanson-Heine, M. W.; Harbach, P. H.; Hauser, A. W.; Hohenstein, E. G.; Holden, Z. C.; Jagau, T.-C.; Ji, H.; Kaduk, B.; Khistyaev, K.; Kim, J.; Kim, J.; King, R. A.; Klunzinger, P.; Kosenkov, D.; Kowalczyk, T.; Krauter, C. M.; Lao, K. U.; Laurent, A. D.; Lawler, K. V.; Levchenko, S. V.; Lin, C. Y.; Liu, F.; Livshits, E.; Lochan, R. C.; Luenser, A.; Manohar, P.; Manzer, S. F.; Mao, S.-P.; Mardirossian, N.; Marenich, A. V.; Maurer, S. A.; Mayhall, N. J.; Neuscamman, E.; Oana, C. M.; Olivares-Amaya, R.; ONeill, D. P.; Parkhill, J. A.; Perrine, T. M.; Peverati, R.; Prociuk, A.; Rehn, D. R.; Rosta, E.; Russ, N. J.; Sharada, S. M.; Sharma, S.; Small, D. W.; Sodt, A.; Stein, T.; Stück, D.; Su, Y.-C.; Thom, A. J.; Tsuchimochi, T.; Vanovschi, V.; Vogt, L.; Vydrov, O.; Wang, T.; Watson, M. A.; Wenzel, J.; White, A.; Williams, C. F.; Yang, J.; Yeganeh, S.; Yost, S. R.; You, Z.-Q.; Zhang, I. Y.; Zhang, X.; Zhao, Y.; Brooks, B. R.; Chan, G. K.; Chipman, D. M.; Cramer, C. J.; Goddard, W. A.; Gordon, M. S.; Hehre, W. J.; Klamt, A.; Schaefer, H. F.; Schmidt, M. W.; Sherrill, C. D.; Truhlar, D. G.; Warshel, A.; Xu, X.; Aspuru-Guzik, A.; Baer, R.; Bell, A. T.; Besley, N. A.; Chai, J.-D.; Dreuw, A.; Dunietz, B. D.; Furlani, T. R.; Gwaltney, S. R.; Hsu, C.-P.; Jung, Y.; Kong, J.; Lambrecht, D. S.; Liang, W.; Ochsenfeld, C.; Rassolov, V. A.; Slipchenko, L. V.; Subotnik, J. E.; Van Voorhis, T.; Herbert, J. M.; Krylov, A. I.; Gill, P. M.; Head-Gordon, M. Advances in molecular quantum chemistry contained in

the Q-Chem 4 program package. *Mol. Phys.* **2015**, *113*, 184–215.

(44) LeTourneau, H. A.; Birsch, R. E.; Korbeck, G.; Radkiewicz-Poutsma, J. L. Study of the Dative Bond in 2-Aminoethoxydiphenyl Borate at Various Levels of Theory: Another Poor Performance of the B3LYP Method for BN Dative Bonds. *J. Phys. Chem. A* **2005**, *109*, 12014–12019, PMID: 16366656.

(45) All energy values listed herein are relative energies, i.e. relative to the lowest energy structure per given method. As such when calculating differences between methods, this is truly a $\Delta\Delta E = \Delta E_{\omega B97x-D} - \Delta E_{M06-2X}$.

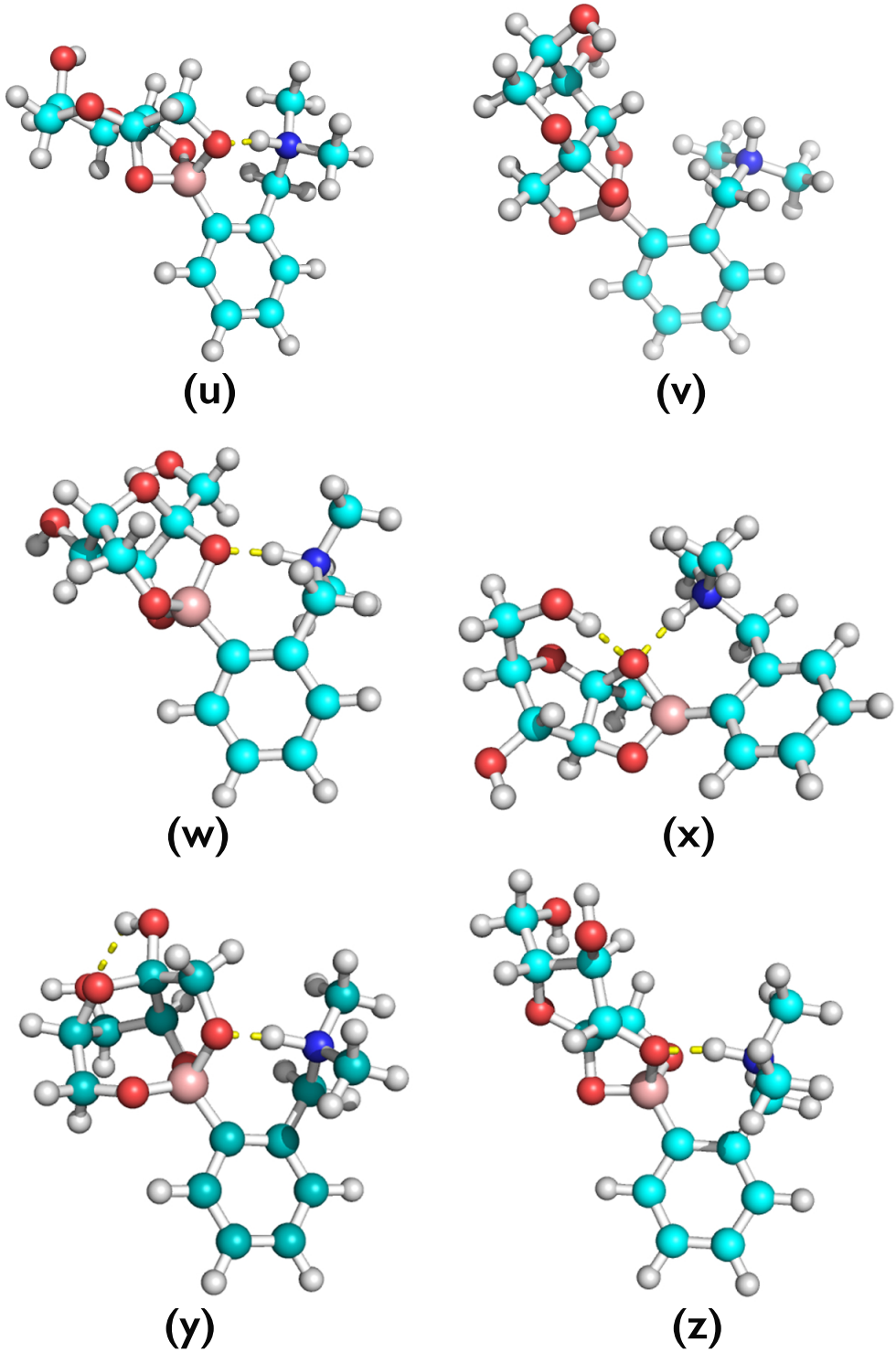
(u)
(v)
(w)
(x)
(y)
(z)

**Table 1:** Relative energies calculated from gas phase geometry optimizations from all 20 fructose receptor binding modes. Energies are listed in kcal·mol$^{-1}$ relative to the lowest energy structure for that functional/basis-set pairs.

| | B3LYP | $\omega$B97x-D | | PBE1PBE | | M06-2X | | PBE | |
|---|---|---|---|---|---|---|---|---|---|
| | 6-31G* | 6-31+G* | 6-311++G** | 6-31+G* | 6-311++G** | 6-31+G* | 6-311++G** | 6-31+G* | 6-311++G** |
| a | 10.06 | 7.64 | 8.22 | 7.80 | 7.99 | 8.65 | 8.59 | 14.42 | 16.39 |
| b | 0.13 | 0.00 | 0.00 | 0.00 | 0.00 | 0.00 | 0.00 | 0.00 | 0.00 |
| c | 8.47 | 1.77 | 2.32 | 5.04 | 5.27 | 2.06 | 1.98 | 16.41 | 18.11 |
| d | 12.86 | 7.93 | 6.96 | 10.78 | 10.92 | 9.48 | 9.36 | 17.79 | 19.73 |
| e | 17.27 | 14.67 | 14.94 | 14.35 | 14.19 | 15.68 | 15.35 | 20.88 | 22.57 |
| f | 5.09 | 5.62 | 5.41 | 5.09 | 4.88 | 5.33 | 5.52 | 6.77 | 5.90 |
| g | 0.00 | 0.05 | 1.54 | 0.14 | 1.54 | 1.51 | 2.75 | 11.67 | 14.30 |
| h | 40.33 | 34.43 | 34.83 | 37.06 | 37.11 | 35.26 | 34.82 | 27.31 | 29.34 |
| i | 10.11 | 6.97 | 8.23 | 8.97 | 10.07 | 6.66 | 7.56 | 20.37 | 22.84 |
| j | 14.30 | 11.46 | 12.40 | 12.42 | 13.22 | 13.32 | 13.83 | 20.55 | 23.02 |
| k | 14.07 | 10.45 | 10.54 | 11.94 | 11.74 | 12.68 | 12.19 | 18.79 | 20.45 |
| l | 37.16 | 32.43 | 33.07 | 35.27 | 36.07 | 32.33 | 32.49 | 38.55 | 40.58 |
| m | 23.40 | 13.54 | 13.47 | 15.11 | 14.57 | 16.72 | 16.16 | 17.82 | 19.06 |
| n | 9.52 | 4.31 | 4.66 | 8.23 | 8.41 | 6.53 | 6.54 | 15.98 | 17.81 |
| o | 26.86 | 9.80 | 10.03 | 12.02 | 11.89 | 12.08 | 11.56 | 23.46 | 24.71 |
| p | 29.75 | 25.65 | 26.11 | 27.49 | 27.62 | 26.45 | 26.15 | 31.61 | 33.29 |
| q | 33.61 | 30.66 | 30.93 | 29.87 | 29.70 | 33.53 | 33.18 | 32.15 | 33.82 |
| r | 35.14 | 30.61 | 30.91 | 31.72 | 31.68 | 32.31 | 32.20 | 36.49 | 38.43 |
| s | 21.84 | 11.78 | 11.97 | 16.26 | 16.17 | 10.09 | 9.65 | 21.01 | 22.27 |
| t | 31.83 | 26.96 | 27.17 | 30.41 | 30.17 | 29.66 | 29.22 | 30.13 | 31.37 |

**Table 2:** Relative energies calculated from SM8 geometry optimizations of the bidentate fructose binding modes. Energies are reported in kcal·mol$^{-1}$ relative to the lowest energy structure. SM8/M06-2X/6-31+G** optimization of **j** was unable to converge, and therefore no energy is reported in that case.

| | $\omega$B97x-D 6-31+G** | M06-2X 6-31+G** |
|---|---|---|
| a | 2.24 | 2.39 |
| b | 0.95 | 1.47 |
| c | 1.31 | 0.00 |
| d | 2.45 | 8.75 |
| e | 6.54 | 5.84 |
| f | 1.87 | 2.69 |
| g | 0.00 | 1.77 |
| h | 21.59 | 21.01 |
| i | 93.49 | 17.12 |
| j | 10.57 | – |
| k | 8.14 | 7.34 |
| l | 23.37 | 22.37 |
| m | 7.41 | 9.67 |
| n | 1.85 | 2.21 |
| o | 9.58 | 9.05 |
| p | 18.99 | 18.05 |
| q | 19.99 | 20.74 |
| r | 23.80 | 25.62 |
| s | 6.84 | 5.00 |
| t | 11.52 | 11.38 |

**Table 3:** Relative energies calculated from SM8 geometry optimizations of all 6 tridentate fructose bound compounds. Energies are listed in kcal·mol$^{-1}$ relative to the lowest energy structure.

| | $\omega$B97x-D 6-31+G** | M06-2X 6-31+G** |
|---|---|---|
| u | 6.58 | 6.33 |
| v | 24.05 | 23.79 |
| w | 0.00 | 0.00 |
| x | 10.72 | 12.67 |
| y | 6.35 | 4.54 |
| z | 25.87 | 26.72 |

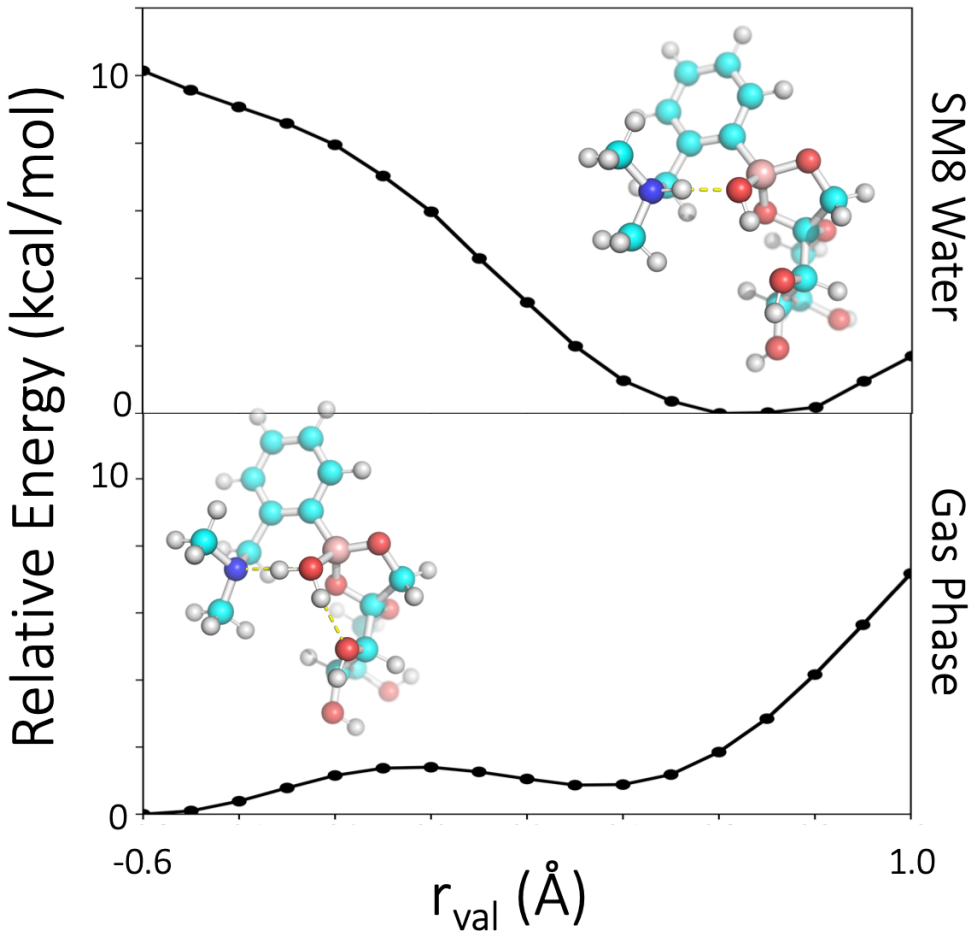


**Figure 10:** TOC-image